NANO · MICRO small
www.small-journal.com

Highly Transparent, Yet Photoluminescent: 2D CdSe/CdS Nanoplatelet-Zeolitic Imidazolate Framework Composites Sensitive to Gas Adsorption

*Lars F. Klepzig, Nils C. Keppler, Dominik A. Rudolph, Andreas Schaate, Peter Behrens, and Jannika Lauth**

In this work, thin composite films of zeolitic imidazolate frameworks (ZIFs) and colloidal two-dimensional (2D) core-crown CdSe/CdS nanoplatelet (NPL) emitters with minimal scattering are formed by a cycled growth method and yield highly transparent coatings with strong and narrow photoluminescence of the NPLs at 546 nm (FWHM: 25 nm) in a solid-state composite structure. The porous ZIF matrix acts as functional encapsulation for the emitters and enables the adsorption of the guest molecules water and ethanol. The adsorption and desorption of the guest molecules is then characterized by a reversable photoluminescence change of the embedded NPLs. The transmittance of the composite films exceeds the values of uncoated glass at visible wavelengths where the NPL emitters show no absorption (>540 nm) and renders them anti-reflective coatings. At NPL absorption wavelengths (440–540 nm), the transmittance of the thin composite film-coated glass lies close to the transmittance of uncoated glass. The fast formation of innovative, smooth NPL/ZIF composite films without pre-polymerizing the colloidal 2D nanostructures first provides a powerful tool toward application-oriented photoluminescence-based gas sensing.

1. Introduction

Innovative photonic applications will feature current progress in material development. Functional materials including colloidal 2D semiconducting nanoplatelets (NPLs) and metal-organic frameworks (MOFs) have been advanced synthetically for different photonic applications such as (directed) light emission, optical waveguiding, and bright and stable photoluminescence (PL).[1,2] Additionally, new functionalities such as fast switching of optical properties can be introduced, if the functional materials are controllable by external triggers such as electric or magnetic fields.[3] In a similar manner, adsorption of analytes to MOFs with high specific surface areas can influence their optical properties and render them excellent candidates for, e.g., gas sensing.[4,5] Consequently, a composite material of NPLs and MOFs is promising to combine the properties of both material classes. There are few synthesis approaches for MOFs in a composite with colloidal semiconductor nanocrystals (NCs) where authors find beneficial effects in the composites such as an increased photoluminescence (PL) quantum yield of polyvinylpyrrolidone (PVP) coated and encapsulated NCs under static conditions already.[6–8]

However, up to now, characterizing a composite film in a dynamically changing gas environment and using the guest-host chemistry of the MOF matrix is missing.

In this work, we show a new composite formed by combining highly photoluminescent colloidal 2D CdSe/CdS core-crown NPLs with ZIF-90 thin films without the need for a PVP

L. F. Klepzig, D. A. Rudolph, J. Lauth
Institute of Physical Chemistry
Leibniz University Hannover
Callinstraße 3A, D-30167 Hannover, Germany
E-mail: jannika.lauth@uni-tuebingen.de

The ORCID identification number(s) for the author(s) of this article can be found under https://doi.org/10.1002/smll.202309533

DOI: 10.1002/smll.202309533

L. F. Klepzig, N. C. Keppler, A. Schaate, P. Behrens, J. Lauth
Cluster of Excellence PhoenixD (Photonics Optics and Engineering – Innovation Across Disciplines)
Leibniz University Hannover
Welfengarten 1A, D-30167 Hannover, Germany

N. C. Keppler, A. Schaate, P. Behrens
Institute of Inorganic Chemistry
Leibniz University Hannover
Callinstraße 9, D-30167 Hannover, Germany

A. Schaate, P. Behrens, J. Lauth
Laboratory of Nano and Quantum Engineering (LNQE)
Leibniz University Hannover
Schneiderberg 39, D-30167 Hannover, Germany

J. Lauth
Institute of Physical Chemistry and Theoretical Chemistry
University of Tübingen
Auf der Morgenstelle 18, D-30167 Tübingen, Germany

coating. The encapsulation of the NPL emitters in the zeolitic imidazolate framework (ZIF) prevents detrimental agglomeration of the NPLs and yields highly transparent composite thin films with narrow PL centered at 546 nm. Such antireflective coatings which can down-convert short wavelength light to longer wavelengths are much sought-after for the improvement of solar cell efficiency.[9] At the same time, the ZIF acts as an active layer. This is shown by the adsorption of guest molecules to the porous ZIF-CdSe/CdS NPL composite film, which changes its relative permittivity and has an influence on both, the refractive index of the ZIF and the PL of the CdSe/CdS NPLs. This behavior enables the composite films to act as gas sensors, e.g., for ethanol or humidity sensing.

2D semiconductor NPLs are nanocrystalline materials that are strongly quantum-confined in their thickness dimension to a few monolayers. NPLs exhibit strong excitonic effects leading to useful optoelectronic properties such as highly efficient and narrow absorption, as well as a PL quantum yield (PLQY) of 90% (with a FWHM of 9 nm at 512 nm).[10] Furthermore, a small Stokes shift and directed emission perpendicular to the 2D plane are observed.[11,12] Colloidal chemistry yields 2D NPLs with uniform thickness and prevents a broadening of the optical features due to thickness dispersion.[13,14] NPLs have shown their potential for optoelectronic applications such as light-emitting diodes, amplified stimulated emission as well as for lasing.[15] Cadmium chalcogenide-based NPLs, especially CdSe, are excellent light-emitting systems at UV-vis wavelengths due to their high PLQY and their photostability.[12] The growth of a lateral crown of CdS around the CdSe core increases the PLQY from 10% up to 90%, while retaining the spectral position and narrow FWHM of the PL.[16,17] Here, we use CdSe/CdS core-crown NPLs ligand exchanged by 3-mercaptoundecanoic acid (MUA) to obtain stable aqueous NPL dispersions which are then used during the encapsulation in thin ZIF layers.

MOFs are highly porous hybrid materials formed by inorganic metal clusters that are bridged by organic linker molecules. The combination of these two building blocks results in the formation of up to 3D crystalline frameworks with high inner surface areas.[18] The materials are interesting for applications in gas storage, gas separation and sensing, and in biomedicine.[5,19] MOF stability is steadily increasing by the development of various thermally and chemically stable subgroups, including ZIFs, which crystallize in topologies that are known from zeolites such as sodalite.[20] Besides, MOFs (including ZIFs) offer a high pore space tunability by the introduction of different functional groups that can be attached to the linker molecules. Polar or non-polar functional groups provide control over the adsorption properties of the framework, which is a powerful tool for sorption-based use.[21]

For applications, composite materials are typically used in their solid-state form. This requires a suitable processing, such as the formation of high-quality thin films with high transparence, low scattering and low deviation of optical properties over a large coated area. Additionally, high quality films are crack-free, dense (no interparticular voids), and smooth. The latter includes that no crystals grow on or out of the surface. Different fabrication methods for MOF thin films have been successfully introduced, including liquid-phase epitaxy (LPE) and cycled direct growth.[22,23] Cycled direct growth is a comparatively fast technique (30 minutes per layer compared to several hours for LPE) that was introduced for the synthesis of ZIF-8 and has also been useful for the synthesis of other ZIFs.[24,25] The highest optical quality of MOF coatings has only been achieved for a few MOFs (HKUST-1 and ZIFs), but without the incorporation of nanomaterials.[23,25–27]

Using colloidal 2D CdSe/CdS NPLs for solid-state application calls for their stable encapsulation inside a matrix.[28,29] Detrimental interactions which lead to a decreased PLQY and non-radiative charge carrier recombination such as charge transfer or FRET can occur between individual NPLs and between the NPLs and the matrix.[6] Suitable matrices must therefore prevent NPL agglomeration while staying inert. For example, the incorporation of NPLs into conductive polymers quenches the PL, while enabling charge carrier separation.[30,31] Typically, a pre-treatment of the nanostructures such as ligand exchange or structure stabilization with an adhesion promoter has to be performed.[6,7,26,32,33] A polymer like PVP is often used to promote adhesion. This process allows for the encapsulation of many different NCs with different functionalities such as metal, metal oxide, or cadmium-based core-shell NCs but has not been used for MOF-NC composite films of optical quality yet.[6,7,32,33] MOFs have proven to be suitable matrices for PVP-coated photoluminescent NCs. Stone et al. have shown that spherical CdSe/CdS NCs in a PVP coating with a thickness of 3–4 nm exhibit increased PLQY in a thin film when encapsulated in a ZIF-8 matrix in comparison to when directly drop-casted without the MOF layer (up to 9.8% and 2.1%, respectively).[6]

Here, we apply a MOF encapsulation for the first time to use its porous nature for influencing the PL of the encapsulated 2D NPL emitters by guest molecules. MUA-stabilized CdSe/CdS NPLs with a thickness of 4 monolayers are combined with thin films of ZIF-8 and ZIF-90 formed by the cycled direct growth method. The surface ligand of the NPLs allows their encapsulation without the need for an adhesion promoter and thus minimizing the distance between the NPLs and the ZIFs. Guest molecules such as water and ethanol alter the PL intensity of the composite thin film already at low NPL loadings. As a result, the film exhibits low absorption and scattering, leading to high transmittance.

2. Results and Discussion

The fabrication process of composite films of CdSe/CdS NPLs encapsulated in ZIF thin films is schematically illustrated in **Figure 1**a. Substrates were first coated with a ZIF-8 thin film using the cycled direct growth method.[23] This ZIF-8 seeding layer is essential for successful subsequent growth of ZIF-90. In a second step, CdSe/CdS NPLs were transferred onto the ZIF-8 film using spin-coating from an aqueous solution. NPL-coated samples were then further coated with a ZIF-90 top layer using a second turn of the cycled direct growth method. The resulting combination of NPLs between two ZIF layers is called "composite film" in the following. In total, only a short fabrication time of ~90 minutes is required for the entire composite film (including drying times). ZIF-90 was chosen as the top-layer because of the linker's polar aldehyde group, adding a higher affinity towards polar molecules to the composite film. This polarity is relevant for the adsorption-based properties of the composite film that will be discussed in the following proof-of-concept gas sensing part.

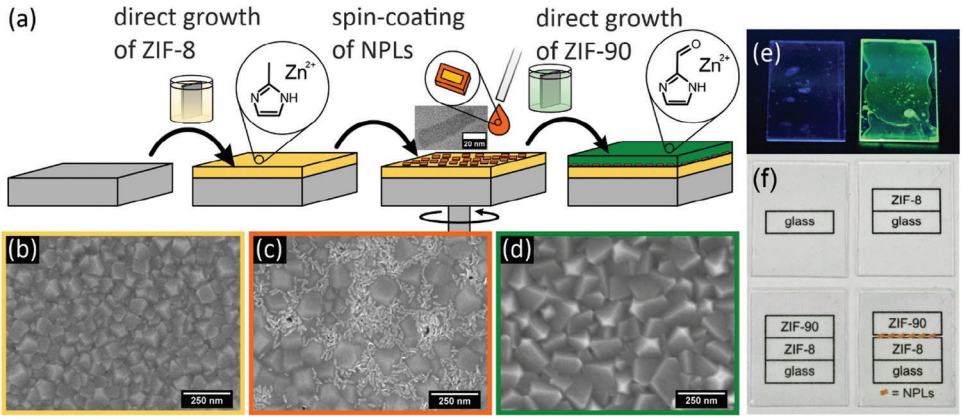

Figure 1. a) Scheme of the fabrication process of ZIF / NPL composite films, with a TEM image of an exemplary single CdSe/CdS NPL with a size of 46 x 13 nm^2. b) SEM images of the ZIF-8 seeding layer before, c) after spin-coating of the NPLs (from an aqueous solution with a concentration of 0.68 µmol/) and d) after coating with a ZIF-90 top layer. e) Photographs of the resulting films under UV light and f) ambient light show that the incorporation of NPLs into the ZIF leads to photoluminescent composite films that retain a high transparence. The films in e) were fabricated on quartz glass without (left) or with (right) NPLs between the ZIF-8 and ZIF-90 layers. The labelling in f) is printed on paper and can be read through the coated glass slides.

An additional advantage compared to other methods is the fabrication at room temperature and at ambient pressure.[34] Scanning electron microscopy (SEM) images of the composite film at different fabrication stages are shown in Figure 1b–d. The ZIF-8 seeding layer (1b) and the final composite film (1d) are polycrystalline, dense, and crack-free. The NPLs are visible in the SEM image of the NPL-coated ZIF-8 seeding layer (1c) and do not affect the growth of the ZIF-90 top layer (see Figure 1d), which completely covers the NPLs and is indistinguishable from a ZIF-90 layer without NPLs (see Figure S1e, Supporting Information). Photographs of thin films under UV light are provided in Figure 1e with both samples being prepared on ZIF-8-coated quartz glass with a ZIF-90 top layer. The left sample was fabricated without spin-coating of NPLs for comparison, while NPLs are included in the right sample. The encapsulation of NPLs in composite films results in visible PL of the sample under UV light. Figure 1f shows photographs of the samples on glass substrates placed on a sheet of paper with printed information about their respective preparation (ZIF-8-coated glass slides with a ZIF-90 top layer and with and without NPLs). All samples show high transparence with the print below the samples clearly visible.

The influence of the concentration of the NPLs in aqueous solution for composite formation was investigated between 0.068 and 2.04 µmol L^{-1} with the aim to achieve a high NPL loading without preventing or hindering the growth of the ZIF-90 top layer encapsulation (SEM images of the samples with different concentrations are provided in Figure S2, Supporting Information). We find that NPL concentrations higher than 0.68 µmol lead to cracks and voids appearing in the ZIF-90 top layer, while at lower concentrations NPLs were only found scarcely (data discussed in the following were acquired with an NPL solution concentration of 0.68 µmol L^{-1}). This concentration corresponds to a low maximum NPL density of 22.7 nmol cm^{-2} (not accounting for losses during spin-coating).

Besides their dense profile (no cracks and voids), thin films of optical quality need to be smooth and homogeneous. To gain more insight into the quality of the NPL/ZIF composite coatings, cross-sectional SEM images are shown in **Figure 2**a. The composite film exhibits a thickness of ~200 nm with no internal voids or crystals growing out of the surface. The ZIF-8 and ZIF-90 layers are well intergrown, again demonstrating that the NPLs do not affect the growth of the ZIF-90 top layer. Note that no individual NPLs are visible in the SEM cross-section between the ZIF layers due to a thickness of individual NPLs of only 1.2 nm.

We characterize the presence of the CdSe/CdS NPLs between the two ZIF layers by X-ray photoelectron spectroscopy (XPS) depth profiling shown in Figure 2b. Here, XPS for the characterization of the film composition is combined with short surface removal phases via sputtering using an argon gas cluster ion beam.[25] A plot of the atomic concentrations of zinc (from ZIF-8 and ZIF-90), cadmium (from CdSe/CdS NPLs), and silicon (from the substrate) depending on the sputtering time is shown. An increasing sputtering time provides information about the atomic concentration at higher film depths. Before and at the beginning of the sputtering process, zinc is the only element present (corresponding to the ZIF-90 top layer). With increasing sputtering time, the cadmium signal increases, while the atomic concentration of zinc decreases. The majority of the NPLs can be observed at the maximum of the cadmium signal. Subsequently, the cadmium signal decreases to zero, indicating that the ZIF-8 seeding layer has been reached, which is confirmed by a re-increasing zinc signal. Further removal of the film surface by sputtering causes the zinc signal to decrease and the silicon signal of the substrate to increase to 100%, indicating the complete removal of the NPL/ZIF film. The XPS results show that the NPLs are well encapsulated between the ZIF layers and can only interact with molecules adsorbed in the ZIF pores.

The composite thin films of CdSe/CdS NPLs in ZIF-90 show high transmittance at UV-Vis wavelengths (see **Figure 3**a; Figure S3 (Supporting Information) for individual absorption properties). The initial transmittance of the glass is ~90% and increases to above 95% due to the growth of the ZIF-8 seeding layer. With a refractive index of 1.36 (between air and glass, 1.00 and 1.50, resp.), the ZIF-8 layer acts as an anti-reflectance coating.[26]

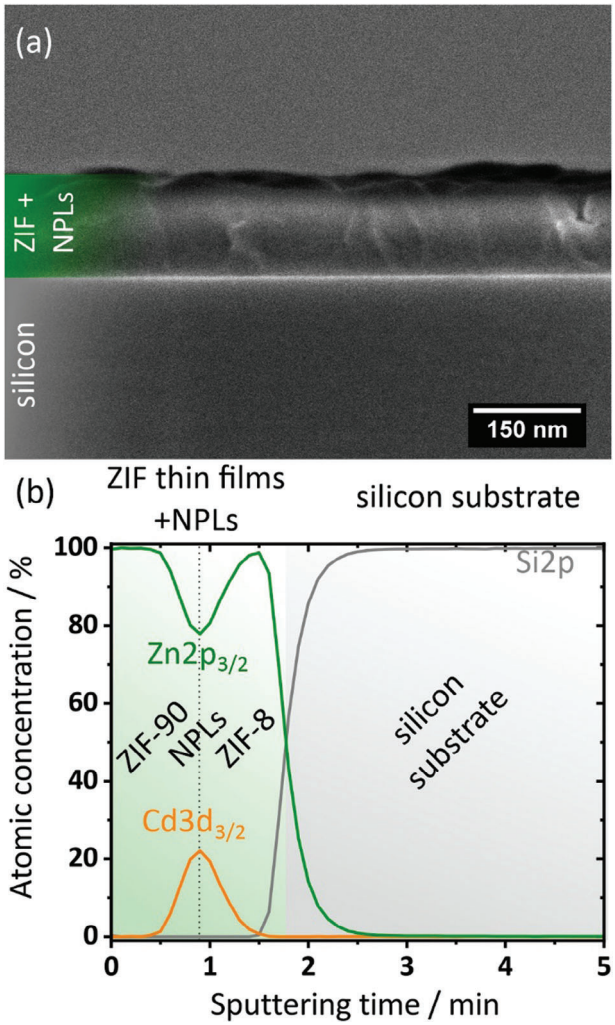

Figure 2. a) Cross-sectional SEM image and b) XPS depth profile of ZIF-8/NPLs/ZIF-90 composites on silicon showing that the composite films are dense and smooth. The NPLs are fully encapsulated in the ZIF layers which can be seen from the Cd signal appearing only in the middle of the composite film.

The 95% transmittance decreases with the growth of the ZIF-90 layer due to scattering at the interface, but still surpasses the values of the glass slide at most wavelengths. The high transmittance is slightly decreased by the addition of the CdSe/CdS NPLs and the formation of the composite film. At 540 nm and shorter wavelengths, the absorption by the NPLs gets apparent for composite samples, increasing at 440 nm where the absorption of the CdS crown is centered (note that the absorption at 380 nm is due to metal impurities caused by the glass substrate).[35] Measuring the absorption of the composite films by using an integrating sphere, we are able to follow the optical features of the films at low optical density of 1 mOD for the heavy-hole and light-hole transition in CdSe, while the transition introduced by the CdS crown exhibits an optical density of 6 mOD (Figure S4, Supporting Information). The absorption of the ZIF-90 coating is below 1 mOD which means that the signal shown in the transmittance measurements can be assigned to scattering.

Figure 3b shows the PL of the CdSe/CdS NPLs directly after synthesis, after the ligand exchange and in the ZIF-90 composite coating respectively. The ligand exchange to MUA is an established route to retain a high PLQY of the NPLs in aqueous solution (35% compared to 70% for NPLs in hexane) and is accompanied by a red-shift (from 513 nm to 542 nm) and slight broadening of the PL (FWHM: 9 nm to 22 nm).[29,36,37]

We find that in the composite film, the PL position and FWHM is nearly retained, only shifting (from 542 nm to 546 nm; FWHM from 22 nm to 25 nm) due to the change of the dielectric constant of the matrix.[38] A rather broad PL background can be attributed to the ZIF-90. The PLQY of the composite film is 8%, well in line with values of 5–10% typically reported for solid-state thin films encapsulating pre-polymerized core-only and core-crown NPLs and NCs.[6,28,29,31,39]

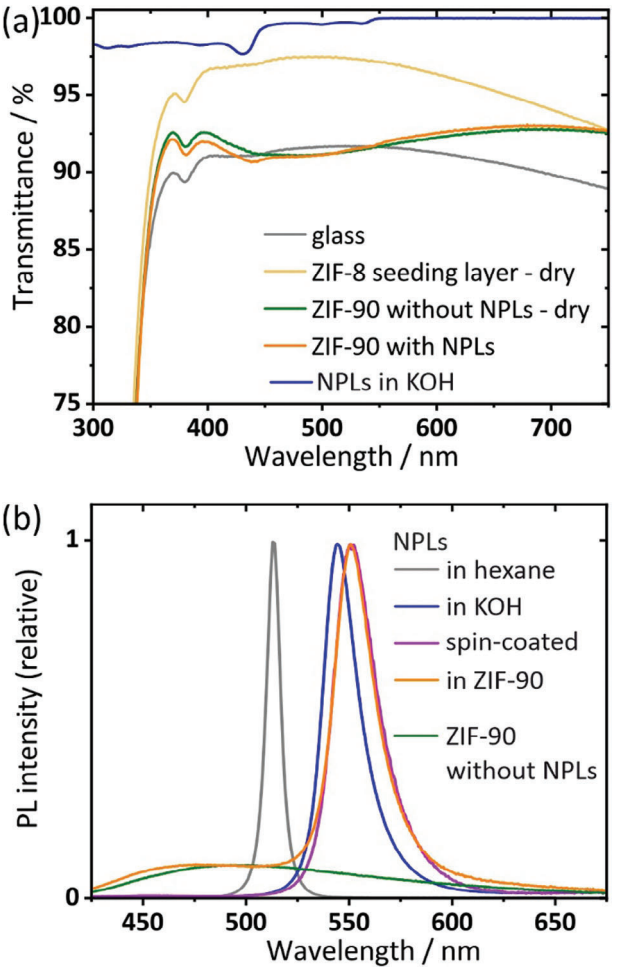

Figure 3. Optical properties of the composite thin films. a) Transmittance of the quartz glass slide, a dispersion of NPLs in KOH, the ZIF-8 seeding layer, a ZIF-90 layer without NPLs as reference and the composite thin film of ZIF-90 with NPLs. The absorption at 380 nm stems from metal impurities in the glass substrate.[33] The transmittance is at first increased due to the ZIF acting as anti-reflectance layer, and decreases with NPLs close to the values of the uncoated glass. b) The PL of the NPLs as synthesized in hexane, red-shifted after the phase transfer to aqueous KOH-solution and in the composite thin film. As a reference, the PL of spin-coated NPLs without the MOF and the PL of a ZIF-90 coating are shown.

An advantage of the porous ZIF-90 layer in the composite film and the omission of a PVP coating is the increased interaction of the NPLs with the ZIF matrix. For example, gas molecules with diameter smaller than the pore size (3.5 Å) could permeate through the ZIF top layer or adsorb in its pores.[40] To characterize the composite film under different gas atmospheres, we use a home-built measurement chamber with quartz glass windows and a gas in- and outlet (see Figure S5, Supporting Information, for detailed description of the setup). Argon was used as the inert gas, and ethanol and water atmospheres were created by bubbling an argon flow through the liquid (reaching at most 5.8 vol% and 2.5 vol%, respectively, as estimated by the vapor pressure). The pressure inside the measurement chamber was always kept at ambient level to avoid pressure-related loss of PL.[41] The PL signal inside the measurement chamber showed a broad background due to light scattered through the transparent gas tubes, with a signal-to-background ratio of 7.5. The signal-to-noise ratio (SNR) was 215 or above, without applying any processing steps.

We find that upon changing the atmosphere from dry to moist argon, the PL signal of the NPL/ZIF composite film increases by 23% (see **Figure 4**a). This change is reversible, and the PL signal decreases again under a dry argon atmosphere. A similar behavior has been described for CdSe/ZnS core-shell NCs and was attributed to the stabilization of a highly emissive surface trap states by water.[42] The interaction has been used for the development of humidity sensors based on CdTe and CdSe/ZnS NCs in combination with non-transparent silica spheres.[43] While spin-coated films of core-crown CdSe/CdS NPLs also show a PL increase (see Figure S6, Supporting Information), their PL signal deteriorates over time. The ZIF-encapsulated NPL sample is stable even after > 30 cycles and 4 h of sampling. The change of the PL signal occurs on the same timescale (<0.5 s) like for spin-coated NPLs only, indicating that the permeation through the ZIF-90 top layer is very fast. Interestingly, when treating the composite films with an ethanol-containing atmosphere, we find a 17% decrease of the PL of the films and an additional blueshift of 0.5 nm (see Figure 4a,b). This does not occur for spin-coated NPLs only, where the PL stays constant under switching between an argon and ethanol-containing atmosphere (Figure S7, Supporting Information). We attribute the PL decrease in the composite film to a change of the dielectric atmosphere of the ZIF matrix due to ethanol adsorption which inevitably leads to an influence on the embedded NPLs. As the desorption of ethanol is highly reversible and rapid, the PL of the NPLs rises again when the matrix returns to the desorbed, ethanol-free, previous dielectric state.[38] The decreasing PL signal starts to occur at an ethanol concentration in the argon stream of 15% (0.375 vol.%), and reaches saturation at 30% onwards (Figure S8, Supporting Information). For comparison we also tested the adsorption of CO_2, which does not considerably change the PL of the pure NPLs or the composite film (see Figure S9, Supporting Information). This is ascribed to the low affinity of CO_2 adsorption on the dielectric properties of ZIFs, which is apparent from the low refractive index change of ZIF-8 and has been reported by us before (when adsorbing ethanol into a ZIF-8 layer, the change of the refractive index is $\Delta n = 0.12$, while the incorporation of CO_2 only leads to a change of $\Delta n = 0.01$).[2]

We follow the PL at its maximum position (546 nm) over 20 min, while the atmosphere is switched repeatedly from pure (dry) argon to ethanol-saturated argon. The PL intensity reproducibly decreases by 17% when switching to the ethanol atmosphere. Switching between argon and ethanol results in a fast and highly reversible PL adjustment without delay, both for adsorption or desorption. The PL intensity is stable over the whole measurement range of 20 min in a single experiment, with a SNR of 100. Multiple (5 and more, > 30 cycles each) experiments have been performed on the same sample without deterioration, with composite coatings showing the same behavior after storage under air for 5 weeks and underlining the high stability of the NPL/ZIF composite films.

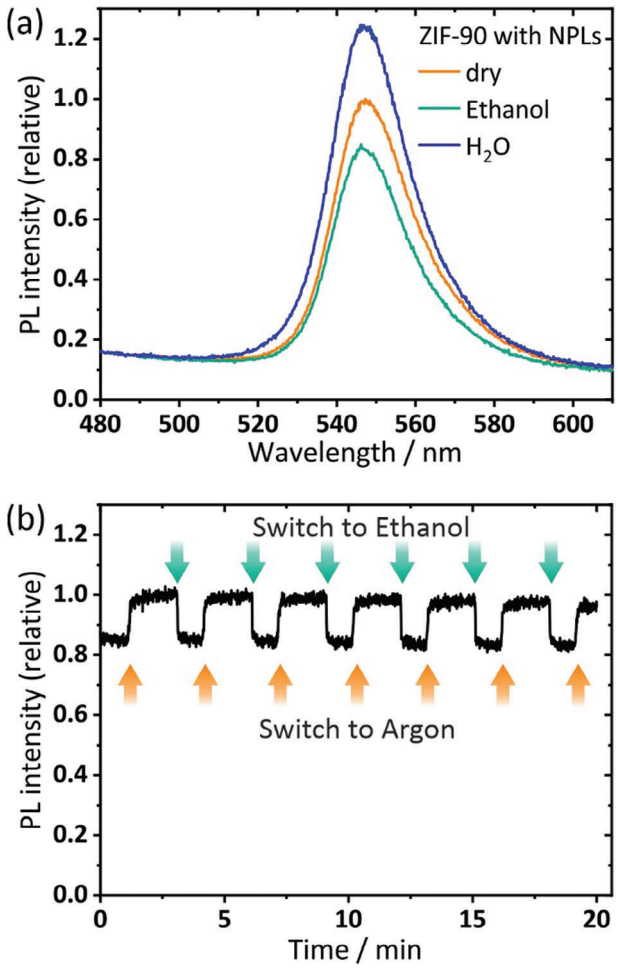

Figure 4. a) PL of the NPL/ZIF composite film under different atmospheres, relative to the composite film PL under dry argon (normalized to 1). Under an ethanol atmosphere, the PL of the NPL/ZIF composite is decreased, while H_2O increases the PL signal. b) The PL intensity is measured at its maximum (546 nm) over 20 min, while the atmosphere is changed repeatedly from argon to argon saturated with ethanol and repeatedly switching the PL intensity.

3. Conclusion

In conclusion, we have shown a new way for the fast synthesis of smooth composite thin films consisting of 2D core-crown CdSe/CdS NPL emitters encapsulated in ZIF films. The presented fabrication method combines two functional materials in

solid-state manner and yields composite films of remarkable optical quality on different substrates such as glass and silicon. These composite films are highly transparent at UV-vis wavelengths, exhibit efficient encapsulation of the emitters by the ZIF films, proven by the stable PL of the embedded NPLs, and additionally offer gas molecule accessibility.

For the first time, such NPL/ZIF composite films have been investigated under a dynamically changing gas environment and making use of the guest-host chemistry of the ZIFs. The new composites allow for an optical sensing of the adsorption and desorption of water and ethanol in the porous structure of ZIF-90 by following the changes in the PL of the embedded NPLs.

This versatility of colloidal nano- and MOF-chemistry opens new ways towards the development of optical components such as PL-based gas sensors and will make our approach easily transferable to other material composites, e.g., to NPLs with a different band gap or to ZIFs with different pore sizes for extended functionality.

4. Experimental Section

Materials: Sodium myristate (≥99%, Sigma-Aldrich), sulfur (99.98%, Sigma-Aldrich), 11-mercaptounecanoic acid (95%, Sigma-Aldrich, MUA), *n*-hexane (≥99%, Sigma-Aldrich), potassium hydroxide (85%, Sigma-Aldrich), cadmium nitrate tetrahydrate (99.999%, Alfa Aesar), selenium (99.999%, 200 mesh, Alfa Aesar), oleic acid (90%, Alfa Aesar), cadmium acetate dihydrate (98%, ABCR), tri-*n*-octylphosphine (97%, ABCR, TOP), zinc(II) nitrate hexahydrate (98%, Sigma-Aldrich), 2-methylimidazole (99%, Sigma-Aldrich, HmIm), imidazole-2-carboxaldehyde (97%, TCI, HImCA), methanol (99.5%, Roth), ethanol (99.8%, dry, Fisher-Scientific), dimethylformamide (99.8%, Sigma-Aldrich, DMF), sulfuric acid (96%, Roth) and hydrogen peroxide (35%, Roth) were used without further purification. 1-octadecene (90%, Sigma Aldrich, ODE) was purified by degassing it at 120 °C under oil pump vacuum ($p \leq 1 \times 10^{-3}$ mbar) for at least 6 h. Afterward, the purified ODE was stored in an air-free glovebox.

Silicon wafers (111-orientation, Sb-doped), purchased from microchemicals, were used for syntheses "on silicon" (for the SEM and XPS measurements). The substrates were cut into pieces of 15 × 15 mm^2. Microscope glass slides were used for syntheses "on glass" (for UV-vis transmittance measurements). Glass substrates were cut into pieces of 21.5 × 26 mm^2. Quartz glass substrates, purchased from Esco Optics, were used for syntheses "on quartz glass" (for absorption and PL measurements). These substrates were delivered in a size of 12 × 25 mm^2. All substrates were cleaned in a freshly prepared mixture of hydrogen peroxide and sulfuric acid (1:2) for 10 min. Afterward, they were rinsed with water once and twice with methanol. Cleaned substrates were directly used for the MOF growth without storage.

Synthesis of Core CdSe and Core-Crown CdSe/CdS Nanoplatelets (NPLs): The synthesis of CdSe NPLs with a thickness of 4 monolayers (ML) was conducted according to Ithurria et al.[13] Cadmium myristate ($Cd(myr)_2$) was synthesized according to Tessier et al.[16] Briefly, in a three-neck flask, a dispersion of 1360 mg (2.4 mmol) $Cd(myr)_2$ and 96 mg (1.2 mmol) Se in 120 mL ODE was prepared and degassed under vacuum for 60 min at 70 °C. Subsequently, the mixture was heated to 240 °C under an argon atmosphere. At 205 °C, 240 mg (1.0 mmol) of $Cd(Ac)_2$ was added and the synthesis was stopped after 12 min by the addition of 8 ml of oleic acid and removal of the heating mantle. The NPLs were purified by the addition of ethanol, centrifugation at 4000 rcf for 10 min and precipitation repeatedly until the supernatant was colorless. The precipitated CdSe NPLs were redispersed in 10 ml hexane.

CdSe/CdS core-crown NPLs were synthesized according to Schlosser et al.[17] Briefly, 1.165 ml of core CdSe NPLs in hexane (c_{Cd} = 40.0 mM, β_{CdSe} = 7.64 mg L^{-1}) were mixed with 180 µl (0.6 mmol) oleic acid, 96 mg (0.4 mmol) $Cd(Ac)_2$ and 8 ml ODE in a three-neck flask. The hexane was carefully removed via oilpump vacuum and the remaining dispersion further degassed for 1 h at 60 °C. Subsequently, the mixture was heated to 240 °C under argon atmosphere, and starting at 215 °C, 6 ml of a 0.05 M solution of sulfur in ODE was injected at a rate of 18 ml h^{-1}. The solution was allowed to further heat up to 240 °C and was kept for an additional 10 min after the completion of the addition. Then it was allowed to cool down to room temperature and the CdSe/CdS NPLs were purified in a similar fashion as for the CdSe core NPLs described above and stored in 2 ml hexane.

The CdSe/CdS core-crown NPLs were transferred to aqueous dispersion according to Kodanek et al.[36] Briefly, 4 mL of a NPL dispersion (c_{Cd} = 20.0 mM) were added to a solution of 0.07 g (0.3 mmol) MUA and 0.04 g (0.7 mmol) KOH in 5 ml of methanol and kept on a shaker overnight. Subsequently, the now colorless top phase of hexane was removed, and the yellow methanol phase centrifuged at 4000 rcf for 10 min. The precipitated CdSe/CdS NPLs were redispersed in 4 mL of aqueous KOH solution (1 mM). For further purification, the centrifugation step was repeated twice by addition of 4 mL ethanol and subsequent redispersion in KOH solution.

Synthesis of Metal-Organic Framework (MOF) Thin Films and MOF/NPLs Composite Thin Films: MOF growth was performed at room temperature (18 °C). Stock solutions of zinc(II) nitrate hexahydrate in methanol (25 mM, denoted as "Zn") and 2-methylimidazole in methanol (50 mM, "HmIm") were prepared, stored at room temperature, and used for several weeks. The solution of imidazole-2-carbaldehyde in DMF (100 mM, "HImCA") was freshly prepared immediately before the synthesis by heating at 70 °C for 45 min. Solutions of HImCA were cooled down to room temperature and were not stored.

All substrates were first coated with a ZIF-8 seeding layer as has been described previously:[23] Equal amounts of Zn and HmIm were mixed in a glass vessel and the substrate was added immediately after mixing. Coating was stopped after 30 min by removing and rinsing of the substrate with methanol, followed by drying in air.

Dried ZIF-8-coated substrates were coated from one side with NPLs from aqueous solution using a spin-coater (Model WS-400BZ-6NPP/AS from Laurell) from one side. Smaller substrates (silicon and quartz glass) were coated by loading 100 µL of the NPL solution (with concentrations ranging from 0.068 µmol L^{-1} to 2.04 µmol L^{-1}) onto the substrate. After initial investigation, typical samples were prepared with a concentration of 0.68 µmol L^{-1}. The NPL solution covered the entire surface. Spinning was performed at 3000 rpm for 60 s. Larger substrates (glass substrates) were coated with 250 µL of the NPL solution using similar spinning parameters.

The ZIF-90 top layer was crystallized on ZIF-8-coated substrates with or without NPLs coated on top, using the cycled direct growth method described above: Equal amounts of Zn and HImCA were mixed in a glass vessel, followed by direct incubation of the substrate. After 30 min, the substrate was removed from the solution, stirred with methanol, and dried in air. The composite film-coated substrates were used directly used for characterization. Coated glass substrates were used for UV-vis measurements, silicon substrates for SEM and XPS investigations, and quartz glass substrates for photoluminescence measurements.

Characterization Methods–UV-Vis Absorption and Photoluminescence (PL) spectroscopy: Dispersions for UV-vis absorption and PL spectroscopy were prepared by dilution in quartz cuvettes with a path length of 10 mm to achieve an optical density of < 0.2 at the first excitonic absorption feature of the NPLs or the excitation wavelength, respectively. Thin film samples on glass were measured using a solid sample holder. Absorption spectra were measured with a Cary 5000 spectrophotometer from Agilent Technologies, equipped with an integrating sphere. The transmittance of the coated and uncoated glass substrates was measured with a Cary 4000 from Agilent Technologies. Steady-state PL emission spectra were acquired on an Edinburgh FLS 1000 UV-vis-NIR PL spectrometer. The PL measurements under different atmospheres using the home-built measurement cell described in Figure S5 (Supporting Information) were performed on a Horiba Fluoromax-4 spectrometer.

Characterization Methods–Atomic Absorption Spectroscopy (AAS): The atomic absorption spectroscopy measurements to determine the Cd ion concentration were performed on a Varian AA140 equipped with an air/acetylene (1.5:3.5) flame atomizer. 5–15 µl of a NPL dispersion were dissolved in *aqua regia* overnight and diluted with 50 mL of Millipore water (R = 18.21 MΩcm) in 50 mL round bottom flasks. At least 5 standard solutions with concentrations between 0 and 2.5 ppm were analyzed for calibration.

Characterization Methods–X-Ray Diffraction (XRD): X-ray diffraction measurements on thin films were carried out with an X-ray diffractometer from STOE working in Bragg-Brentano geometry. An Iso-Debyeflex 3003 was used for the generation of X-rays at 40 kV and 30 mA, delivering $CuK_{\alpha 1}$ radiation. Measurements were carried out between 5 and 30° 2θ with a step size of 0.02° 2θ and a measurement time of 8 s per step.

Characterization Methods–Scanning Electron Microscopy (SEM): Coated silicon samples were prepared for SEM by fixing the specimen samples on SEM metal substrate holders using carbon tape. Electrical contact of the thin films was ensured by using a silver conductive layer and by sputtering the samples with a thin layer of gold. Most SEM images were recorded with a Regulus SU8200 (Hitachi). Cross-sectional SEM images were recorded by fixing the substrates in a substrate holder enabling to fix them with the fracture edge upside. Images were taken at 2 kV, 10 µA and a working distance of 3 mm.

Characterization Methods–Transmission Electron Microscopy (TEM): TEM was carried out on a FEI Tecnai G2 F20 transmission microscope equipped with a field emission gun operating at 200 kV. The CdSe/CdS NPL sample was prepared by drop casting a diluted dispersion onto a carbon coated copper grid (300 mesh) from Quantifoil.

Characterization Methods–X-Ray Photoelectron Spectroscopy (XPS): The XPS depth profiling was performed with a PHI VersaProbe III (Physical Electronics GmbH) XPS system. The oxidation state of the material was analyzed using microfocused Al K_α X-rays (1486.7 eV, 50 W, 15 kV) with an X-ray spot size of 200 µm in diameter; dual-beam charge neutralization (a 1 V electron beam and a 7 V Ar^+ ion beam) was applied during measurements. For the sputter phase (6 s for every sputtering step), a 20 kV argon gas cluster ion beam with a sputter raster size of 2 mm x 2 mm was used. The acquired data were processed and evaluated using the MultiPak Software (ULVAC-PHI).

Supporting Information

Supporting Information is available from the Wiley Online Library or from the author.

Acknowledgements

L.F.K. and N.C.K. contributed equally to this work. The authors thank André Niebur for TEM measurements, and the Laboratory of Nano and Quantum Engineering (LNQE) in Hannover for access to the TEM. The authors thank Nadja Bigall and Dirk Dorfs for access to the UV-vis-NIR absorption and emission spectrometers. The authors were grateful for funding by the Deutsche Forschungsgemeinschaft (DFG, German Research Foundation) under Germany's Excellence Strategy within the Cluster of Excellence PhoenixD (EXC 2122, Project ID 390833453). J.L. gratefully acknowledges additional funding by the Caroline Herschel program of the Leibniz Universität Hannover.

Open access funding enabled and organized by Projekt DEAL.

Conflict of Interest

The authors declare no conflict of interest.

Data Availability Statement

The data that support the findings of this study are available from the corresponding author upon reasonable request.

Keywords

colloidal nanoplatelets, composite materials, encapsulation, gas sensitivity, metal-organic frameworks, mof thin films, photoluminescence

Received: November 19, 2023
Published online:

[1] a) C. Palacios-Berraquero, M. Barbone, D. M. Kara, X. Chen, I. Goykhman, D. Yoon, A. K. Ott, J. Beitner, K. Watanabe, T. Taniguchi, A. C. Ferrari, M. Atatüre, *Nat. Commun.* **2016**, *7*, 12978; b) I. Suarez, R. Munoz, V. Chirvony, J. P. Martinez-Pastor, M. Artemyev, A. Prudnikau, A. Antanovich, A. Mikhailov, *IEEE J. Select. Topics Quantum Electron.* **2017**, *23*, 1; c) T. Erdem, H. V. Demir, *Nanophotonics* **2016**, *5*, 74.

[2] L. Zheng, N. Keppler, H. Zhang, P. Behrens, B. Roth, *Adv. Mater. Technol.* **2022**, *7*, 2200395.

[3] a) A. W. Achtstein, A. V. Prudnikau, M. V. Ermolenko, L. I. Gurinovich, S. V. Gaponenko, U. Woggon, A. V. Baranov, M. Y. Leonov, I. D. Rukhlenko, A. V. Fedorov, M. V. Artemyev, *ACS Nano* **2014**, *8*, 7678; b) Y. Zhu, H. I. Elim, Y.-L. Foo, T. Yu, Y. Liu, W. Ji, J.-Y. Lee, Z. Shen, A. T. S. Wee, J. T. L. Thong, C. H. Sow, *Adv. Mater.* **2006**, *18*, 587; c) Z. Chai, X. Hu, F. Wang, X. Niu, J. Xie, Q. Gong, *Adv. Opt. Mater.* **2017**, *5*, 1600665; d) Q.-F. Dai, H.-D. Deng, W.-R. Zhao, J. Liu, L.-J. Wu, S. Lan, A. V. Gopal, *Opt. Lett.* **2010**, *35*, 97.

[4] M. Chern, J. C. Kays, S. Bhuckory, A. M. Dennis, *Methods Appl. Fluoresc.* **2019**, *7*, 012005.

[5] K.-J. Kim, P. Lu, J. T. Culp, P. R. Ohodnicki, *ACS Sens.* **2018**, *3*, 386.

[6] A. E. B. S. Stone, S. Irgen-Gioro, R. López-Arteaga, J. T. Hupp, E. A. Weiss, *Chem. Mater.* **2022**, *34*, 1921.

[7] G. Lu, S. Li, Z. Guo, O. K. Farha, B. G. Hauser, X. Qi, Y. Wang, X. Wang, S. Han, X. Liu, J. S. Duchene, H. Zhang, Q. Zhang, X. Chen, J. Ma, S. C. J. Loo, W. D. Wei, Y. Yang, J. T. Hupp, F. Huo, *Nat. Chem.* **2012**, *4*, 310.

[8] K. Kumagai, T. Uematsu, T. Torimoto, S. Kuwabata, *Chem. Mater.* **2021**, *33*, 1607.

[9] a) K. Matsumoto, M. Hagiwara, S. Fujihara, *Coatings* **2017**, *7*, 74; b) S. Tanaka, S. Fujihara, *Langmuir* **2011**, *27*, 2929; c) K. Baryshnikova, D. Gets, T. Liashenko, A. Pushkarev, I. Mukhin, Y. Kivshar, S. Makarov, *Laser Photonics Rev.* **2020**, *14*, 2000338; d) J. Y. Huang, G. T. Fei, S. H. Xu, B. Wang, *Composites, Part B* **2023**, *251*, 110486.

[10] a) F. Manteiga Vázquez, Q. Yu, L. F. Klepzig, L. D. A. Siebbeles, R. W. Crisp, J. Lauth, *J. Phys. Chem. Lett.* **2021**, *12*, 680; b) C. Bouet, M. D. Tessier, S. Ithurria, B. Mahler, B. Nadal, B. Dubertret, *Chem. Mater.* **2013**, *25*, 1262; c) L. Guillemeney, L. Lermusiaux, G. Landaburu, B. Wagnon, B. Abécassis, *Commun. Chem.* **2022**, *5*, 7; d) S. M. Tenney, V. Vilchez, M. L. Sonnleitner, C. Huang, H. C. Friedman, A. J. Shin, T. L. Atallah, A. P. Deshmukh, S. Ithurria, J. R. Caram, *J. Phys. Chem. Lett.* **2020**, *11*, 3473.

[11] a) L. F. Klepzig, L. Biesterfeld, M. Romain, A. Niebur, A. Schlosser, J. Hübner, J. Lauth, *Nanoscale Adv* **2022**, *4*, 590; b) R. Scott, J. Heckmann, A. V. Prudnikau, A. Antanovich, A. Mikhailov, N. Owschimikow, M. Artemyev, J. I. Climente, U. Woggon, N. B. Grosse, A. W. Achtstein, *Nat. Nanotechnol.* **2017**, *12*, 1155; c) X. Liu, F. Li, M. Hohgardt, L. F. Klepzig, M. M. Willich, H.-A. Christ, A. Schaate, P. Behrens, J. Lauth, H. Menzel, P. J. Walla, *H. Menzel Macromol. Mater. Eng.* **2023**, *308*, 2300027.

[12] S. Ithurria, B. Dubertret, *J. Am. Chem. Soc.* **2008**, *130*, 16504.

[13] S. Ithurria, M. D. Tessier, B. Mahler, R. P. S. M. Lobo, B. Dubertret, A. l. L. Efros, *Nat. Mater.* **2011**, *10*, 936.

[14] A. B. Pun, S. Mazzotti, A. S. Mule, D. J. Norris, *Acc. Chem. Res.* **2021**, *54*, 1545.

[15] a) B. Guzelturk, Y. Kelestemur, M. Olutas, S. Delikanli, H. V. Demir, *ACS Nano* **2014**, *8*, 6599; b) Z. Chen, B. Nadal, B. Mahler, H. Aubin, B. Dubertret, *Adv. Funct. Mater.* **2014**, *24*, 295; c) Y. Yang, C. Zhang, X. Qu, W. Zhang, M. Marus, B. Xu, K. Wang, X. W. Sun, *IEEE Trans. Nanotechnology* **2019**, *18*, 220; d) J. J. Geuchies, R. Dijkhuizen, M. Koel, G. Grimaldi, I. Du Fossé, W. H. Evers, Z. Hens, A. J. Houtepen, *ACS Nano* **2022**, *16*, 18777; e) R. Tomar, A. Kulkarni, K. Chen, S. Singh, D. Van Thourhout, J. M. Hodgkiss, L. D. A. Siebbeles, Z. Hens, P. Geiregat, *J. Phys. Chem. C* **2019**, *123*, 9640; f) R. Duan, Z. Zhang, L. Xiao, X. Zhao, Y. T. Thung, L. Ding, Z. Liu, J. Yang, V. D. Ta, H. Sun, *Adv. Mater.* **2022**, *34*, 2108884; g) M. Sak, N. Taghipour, S. Delikanli, S. Shendre, I. Tanriover, S. Foroutan, Y. Gao, J. Yu, Z. Yanyan, S. Yoo, C. Dang, H. V. Demir, *Adv. Funct. Mater.* **2020**, *30*, 1907417; h) S. Spelthann, D. H. Chau, L. F. Klepzig, D. A. Rudolph, M. Chemnitz, S. Junaid, D. Ristau, M. A. Schmidt, J. Lauth, M. Steinke, *arXiv preprint* **2023**; i) Y. Kelestemur, Y. Shynkarenko, M. Anni, S. Yakunin, M. L. De Giorgi, M. V. Kovalenko, *ACS Nano* **2019**, *13*, 13899.

[16] M. D. Tessier, P. Spinicelli, D. Dupont, G. Patriarche, S. Ithurria, B. Dubertret, *Nano Lett.* **2014**, *14*, 207.

[17] A. Schlosser, R. T. Graf, N. C. Bigall, *Nanoscale Adv* **2020**, *2*, 4604.

[18] a) J. H. Cavka, S. Jakobsen, U. Olsbye, N. Guillou, C. Lamberti, S. Bordiga, K. P. Lillerud, *J. Am. Chem. Soc.* **2008**, *130*, 13850; b) I. M. Hönicke, I. Senkovska, V. Bon, I. A. Baburin, N. Bönisch, S. Raschke, J. D. Evans, S. Kaskel, *Angew. Chem., Int. Ed.* **2018**, *57*, 13780.

[19] a) X. Ge, R. Wong, A. Anisa, S. Ma, *Biomaterials* **2022**, *281*, 121322; b) Y. Ji, L. Ding, Y. Cheng, H. Zhou, S. Yang, F. Li, Y. Li, *J. Phys. Chem. C* **2017**, *121*, 24104; c) Q. Qian, P. A. Asinger, M. J. Lee, G. Han, K. Mizrahi Rodriguez, S. Lin, F. M. Benedetti, A. X. Wu, W. S. Chi, Z. P. Smith, *Chem. Rev.* **2020**, *120*, 8161.

[20] K. S. Park, Z. Ni, A. P. Côté, J. Y. Choi, R. Huang, F. J. Uribe-Romo, H. K. Chae, M. O'keeffe, O. M. Yaghi, *Proc. Natl. Acad. Sci. USA* **2006**, *103*, 10186.

[21] a) H. Hahm, K. Yoo, H. Ha, M. Kim, *Inorg. Chem.* **2016**, *55*, 7576; b) G. E. Cmarik, M. Kim, S. M. Cohen, K. S. Walton, *Langmuir* **2012**, *28*, 15606.

[22] J. Liu, C. Wöll, *Chem. Soc. Rev.* **2017**, *46*, 5730.

[23] G. Lu, J. T. Hupp, *J. Am. Chem. Soc.* **2010**, *132*, 7832.

[24] a) J.-L. Zhuang, A. Terfort, C. Wöll, *Coord. Chem. Rev.* **2016**, *307*, 391; b) A. Knebel, P. Wulfert-Holzmann, S. Friebe, J. Pavel, I. Strauß, A. Mundstock, F. Steinbach, J. Caro, *Chem.-Eur. J.* **2018**, *24*, 5728.

[25] N. C. Keppler, J. Fricke, A. Schaate, A. Hannebauer, K. D. J. Hindricks, S. Zailskas, P. Behrens, *Cryst. Growth Des.* **2022**, *22*, 7008.

[26] N. C. Keppler, K. D. J. Hindricks, P. Behrens, *RSC Adv.* **2022**, *12*, 5807.

[27] Z.-G. Gu, A. Pfriem, S. Hamsch, H. Breitwieser, J. Wohlgemuth, L. Heinke, H. Gliemann, C. Wöll, *Microporous Mesoporous Mater.* **2015**, *211*, 82.

[28] C. Lesser, M. Gao, S. Kirstein, *Mater. Sci. Eng., C* **1999**, *9*, 159.

[29] F. Li, L. F. Klepzig, N. Keppler, P. Behrens, N. C. Bigall, H. Menzel, J. Lauth, *Langmuir* **2022**, *38*, 11149.

[30] B. Guzelturk, F. Menk, K. Philipps, Y. Kelestemur, M. Olutas, R. Zentel, H. V. Demir, *J. Phys. Chem. C* **2016**, *120*, 3573.

[31] D. I. Shiman, V. Sayevich, C. Meerbach, P. A. Nikishau, I. V. Vasilenko, N. Gaponik, S. V. Kostjuk, V. Lesnyak, *ACS Appl. Nano Mater* **2019**, *2*, 956.

[32] A. Wolf, L. Diestel, F. Lübkemann, T. Kodanek, T. Mohamed, J. Caro, D. Dorfs, *Chem. Mater.* **2016**, *28*, 7511.

[33] M. Niemeyer, P. Bessel, P. Rusch, R. Himstedt, D. Kranz, H. Borg, N. C. Bigall, D. Dorfs, *ChemNanoMat* **2022**, *8*, 202200169.

[34] a) O. Shekhah, H. Wang, S. Kowarik, F. Schreiber, M. Paulus, M. Tolan, C. Sternemann, F. Evers, D. Zacher, R. A. Fischer, C. Wöll, *J. Am. Chem. Soc.* **2007**, *129*, 15118; b) C. Zhang, Y. Zhao, Y. Li, X. Zhang, L. Chi, G. Lu, *Chem. Asian J.* **2016**, *11*, 207.

[35] G. H. Sigel, *JR. in Treatise on Materials Science & Technology*, Elsevier, xx **1977**, 5.

[36] T. Kodanek, H. M. Banbela, S. Naskar, P. Adel, N. C. Bigall, D. Dorfs, *Nanoscale* **2015**, *7*, 19300.

[37] B. Mahler, B. Nadal, C. Bouet, G. Patriarche, B. Dubertret, *J. Am. Chem. Soc.* **2012**, *134*, 18591.

[38] E. C. Niculescu, *Superlattices Microstruct.* **2012**, *51*, 814.

[39] a) N. J. L. K. Davis, J. R. Allardice, J. Xiao, A. Karani, T. C. Jellicoe, A. Rao, N. C. Greenham, *Mater. Horiz.* **2019**, *6*, 137; b) S. Naskar, J. F. Miethe, S. Sánchez-Paradinas, N. Schmidt, K. Kanthasamy, P. Behrens, H. Pfnür, N. C. Bigall, *Chem. Mater.* **2016**, *28*, 2089.

[40] W. Morris, C. J. Doonan, H. Furukawa, R. Banerjee, O. M. Yaghi, *J. Am. Chem. Soc.* **2008**, *130*, 12626.

[41] M. Lorenzon, S. Christodoulou, G. Vaccaro, J. Pedrini, F. Meinardi, I. Moreels, S. Brovelli, *Nat. Commun.* **2015**, *6*, 6434.

[42] K. Pechstedt, T. Whittle, J. Baumberg, T. Melvin, *J. Phys. Chem. C* **2010**, *114*, 12069.

[43] a) B. Yuan, X. Zhang, J. Yu, L. Zhou, B. Luo, Y. Liu, R. Chen, *Adv. Materials Inter.* **2022**, *9*, 2201366; b) P. Xia, Q. Shou, T. Wang, G. Yang, H. Li, Q. Li, Y. Chen, T. Xie, J. Huang, X. Xing, *Opt. Lett.* **2022**, *47*, 2674